LBL-29802
Preprint

Lawrence Berkeley Laboratory
UNIVERSITY OF CALIFORNIA

Materials & Chemical Sciences Division

Submitted to Journal of the Optical Society of America B

Electronic Coherent Anti-Stokes Raman Spectroscopy in CeF_3

D. Piehler

November 1990

Prepared for the U.S. Department of Energy under Contract Number DE-AC03-76SF00098

DISCLAIMER

LBL-29802

Electronic coherent anti-Stokes Raman spectroscopy in CeF_3

David Piehler

Department of Physics, University of California, Berkeley, California 94720
and
Materials and Chemical Sciences Division, Lawrence Berkeley Laboratory,
Berkeley, California 94720

This work was supported by the Director, Office of Energy Research, Office of Basic Energy Sciences, Chemical Sciences Division of the U. S. Department of Energy under Contract No. DE-AC03-76SF00098.

Electronic coherent anti-Stokes Raman spectroscopy in CeF_3

David Piehler

Department of Physics, University of California, Berkeley, California 94720
and
Materials and Chemical Sciences Division, Lawrence Berkeley Laboratory, Berkeley, California 94720

Abstract

This paper reports the coherent anti-Stokes Raman spectra (CARS) of electronic states of the Ce^{3+} ion in a CeF_3 crystal at 3.8 K. CARS resonances involving the ground state of the $^2F_{5/2}$ manifold and the Stark components of the $^2F_{7/2}$ manifold at 2161 cm^{-1} and 2239 cm^{-1} have been detected. Measurements were made with both visible ($\lambda_1 \approx 476$ nm, $\lambda_2 =$ 532 nm) and near ultraviolet ($\lambda_1 = 355$ nm, $\lambda_2 \approx 385$ nm) lasers. The enhancement of the third-order susceptibility due to the electronic transitions, $|\chi^{(3)R}/\chi^{(3)NR}|_{max}$, is as great as 4.8. This represents an order of magnitude increase over singly resonant electronic CARS experiments in other rare earth crystals. The CARS data also yielded accurate measurement of the Ce^{3+} electronic Raman cross sections. In the visible region, σ_{zz} (2161 cm^{-1}) = $(5.0\pm1.1) \times 10^{-30}$ cm^2, and σ_{zz} (2239 cm^{-1}) = $(1.9\pm0.7) \times 10^{-30}$ cm^2. Both the absolute magnitude and dispersion of $|\chi^{(3)R}|_{max}$ could be calculated by modeling the virtual intermediate states as a single degenerate $5d$ state at 45000 cm^{-1}.

I. Introduction

Coherent anti-Stokes Raman spectroscopy (CARS) is a four-wave mixing process which provides essentially the same information as spontaneous Raman scattering. Both processes use visible light to locate and determine the symmetries of low-lying (infrared) energy levels. CARS has advantages over spontaneous scattering since the signal may have a large ($> 10^6$) dynamic range, the signal is intense and directional, and it allows excellent florescence rejection.

Unlike CARS involving vibrational transitions, CARS involving the $4f^n$ electronic states of rare earth ions in insulating crystals has shown only limited success [1, 2]. This is mainly due to the small cross sections for spontaneous electronic Raman scattering in rare earth crystals. The magnitude of the resonant part of the third-order susceptibility which describes the CARS process, $\chi^{(3)R}$, is roughly proportional to the product of the spontaneous Raman cross section and the number density of ions. In fully concentrated rare earth crystals, $\chi^{(3)R}$ is often so small that resonances are greatly obscured by $\chi^{(3)NR}$, the nonresonant susceptibility, which can be orders of magnitude larger. This effect is compounded for dilute rare earth crystals. The quantity $C = |\chi^{(3)R}/\chi^{(3)NR}|_{max}$ may be considered to be a figure of merit for CARS experiments. Systems with higher C yield better information. Previous experiments in $Tb_3Al_5O_{12}$ [1] and PrF_3 [2] at low temperatures gave values of C no higher than 0.5.

$\chi^{(3)R}$ will increase as the frequencies of the input lasers approach the strong $4f \rightarrow 5d$ electric dipole transitions of the rare earth ions. Among the trivalent rare earth ions, Ce^{3+} with its single $4f$ electron is not only the simplest to analyze, but also has the lowest excited $5d$ configuration. In a doubly resonant CARS experiment [3], Piehler and Edelstein demonstrated that strong electronic CARS resonances ($C > 11$) could be detected in a dilute crystal (0.06 mol % Ce^{3+} doped into $LuPO_4$) only when the anti-Stokes signal was nearly resonant with the onset of the lowest $5d$ level at 30460 cm^{-1}. This paper reports

the observation of singly resonant electronic CARS in a fully concentrated cerium crystal – CeF_3. In CeF_3, the levels of $5d$ configuration range from about 40000 to 50000 cm^{-1}. This rather low energy $5d$ configuration is responsible for a relatively large electronic Raman cross section. This large cross section leads to a high figure of merit, and the detection of strong CARS resonances ($C > 1$) with visible lasers should be possible.

In the CeF_3 crystal, the spectra of both the ground $4f$ and excited $5d$ configurations [4–12] as well as the linear [13] and nonlinear [14, 15] refractive indices have been characterized. From the linear and nonlinear refractive indices, $\chi^{(3)NR}$ may be estimated. Experimental CARS measurements yield $|\chi^{(3)R}/\chi^{(3)NR}|_{max}$ which leads to an absolute measurement of $|\chi^{(3)R}|_{max}$. The spontaneous Raman cross section may be derived from $|\chi^{(3)R}|_{max}$.

In the appendix, $|\chi^{(3)R}|_{max}$ is calculated using the Axe [16] theory of two-photon processes which follows the Judd-Ofelt [17, 18] theory for $4f^n \rightarrow 4f^n$ single photon intensities. Both involve summations over intermediate states of excited electronic configurations whose parity is opposite that of the ground $4f^n$ configuration. In both theories, calculations are simplified by assuming that all electronic states within each excited configuration are degenerate in energy. *Absolute* two-photon intensities may be calculated if the energies, $\hbar\omega_{nl}$, of the excited nl configurations and radial integrals $|\langle 4f|r|nl\rangle|$ are known. Usually, the $4f^{(n-1)}5d^1$ configuration is expected to make the major contribution to the intensity since other excited states of opposite parity (*e. g.* $4f^{(n-1)}ng^1$) are too high in energy to contribute appreciably. Most previous work [19] on two-photon $4f^n \rightarrow 4f^n$ transitions (two-photon absorption and electronic Raman scattering) in rare earth crystals measured *relative* intensities, and application of the Axe theory did not require knowledge of $\hbar\omega_{5d}$ and $|\langle 4f|r|5d\rangle|$. Chase and Payne [20], however, measured absolute two-photon absorption cross sections of the Nd^{3+} ion in YAG and $LiYF_4$ crystals. They found a significant difference in cross sections between the host crystals which suggested

that $\hbar\omega_{5d}$ and $|\langle 4f|r|5d\rangle|$ differ from their free ion values and vary according to the host crystal.

For most trivalent rare earth crystals, the $4f^{(n-1)}5d^1$ configuration lies in the vacuum ultraviolet. When the ion is introduced into a crystal lattice, these states are often well above the crystal band gap, and experimental evaluation of $\hbar\omega_{5d}$ and $|\langle 4f|r|5d\rangle|$ is impossible. For Ce^{3+} systems, however, the states of the $5d$ configuration are usually in the 20000 to 60000 cm^{-1} range, and $\hbar\omega_{5d}$ and $|\langle 4f|r|5d\rangle|$ may be derived from absorption measurements. This allows an independent test of the Axe theory, which uses the same approximations as the more familiar Judd-Ofelt theory. (The quantities which characterize absolute single photon intensities in the Judd-Ofelt theory are related to the odd parity components of the crystal field, and cannot be measured in an independent experiment.)

Williams *et al.* [21, 22] studied the Ce^{3+} ion in $LuPO_4$, and related the observed absolute electronic Raman cross sections to observed $4f \rightarrow 5d$ oscillator strengths and a reduction of $|\langle 4f|r|5d\rangle|$ relative to its free ion value.

In this paper, both $|\langle 4f|r|5d\rangle|$ and $\hbar\omega_{5d}$ for CeF_3 have been derived from $4f \rightarrow 5d$ absorption measurements. $|\chi^{(3)R}|_{max}$ is then calculated from the Axe theory, and compared with experimental measurements.

There are two main conclusions to be drawn from this paper. One is that the electronic CARS signals in rare earth crystals may be significantly greater than reported in earlier experiments. Additionally, both the magnitude and dispersion of $|\chi^{(3)R}|_{max}$ agree with the predictions of the Axe theory in which the states of the excited $5d$ configuration are the dominate intermediate states.

II. Electronic Structure and Optical Properties of CeF_3

The crystal CeF_3 (like LaF_3) has the trigonal space group D^4_{3d} [23, 24]. The site symmetry of the Ce^{3+} ion is C_2 with three two-fold C_2 axes perpendicular to the three-fold C_3 crystal axis. All Ce^{3+} ions experience the same C_2 crystal field, however there are three distinct C_2 axes. The three-fold crystal axis defines the z direction and the x and y axes are chosen arbitrarily. The number density of Ce^{3+} ions is 1.88×10^{22} cm^{-3} [25].

The spin-orbit interaction splits the lowest energy configuration, $4f$, into two multiplets $^2F_{7/2}$ and $^2F_{5/2}$ separated by about 2200 cm^{-1}. The $^2F_{5/2}$ multiplet is the ground state. A C_2 crystal field should split the $J = 7/2$ multiplet into a manifold of four Stark components, and the $J = 5/2$ state into three Stark components. The $5d$ electron experiences a substantially larger crystal field, and along with the spin-orbit interaction, the C_2 crystal field should split the $5d$ configuration into five levels. The irreducible representation of the double group of C_2 labels the levels which are all Kramers doublets. Each level has the same symmetry label, and there are no selection rules for radiative transitions.

Buchanan *et al.* [5] first measured the levels of the $4f$ configuration in CeF_3 by infrared absorption at liquid helium temperature. They located the four Stark components of the $^2F_{7/2}$ manifold in the 2400 cm^{-1} range with the highest two levels having quite broad (~ 30 cm^{-1}) linewidths. Higher temperature spectra indicated possible absorption from an electronic level at ~ 150 cm^{-1}, but a third $^2F_{5/2}$ level was not found. Most recently, experiments by Gerlinger and Schaak [6] have resolved the problem of the missing $^2F_{5/2}$ Stark component. By coincidence, the Stark components of the $^2F_{5/2}$ manifold are nearly resonant with the optical phonons of the crystal. This results in a hybridization of the electronic states of the Ce^{3+} ion with the phonon states to form new vibronic states. The low temperature Raman spectrum in this region shows broad (~ 100 cm^{-1}) features, where one might expect separate narrow Raman lines for the optical phonons and the electronic

levels. Gerlinger and Schaak located the four Stark components of the $^2F_{7/2}$ manifold by electronic Raman scattering. These levels are listed in Table 1.

In 1934, Van Velck and Hebb [4] studied Faraday rotation in CeF_3, and assigned the broad absorption at ~ 250 nm to the $4f \rightarrow 5d$ transition. The $5d$ configuration of $Ce_xLa_{(1-x)}F_3$ has been studied with various Ce^{3+} concentrations [7–12]. All investigations showed five $5d$ levels with the absorption peaks at roughly the same energies. As the concentration of Ce^{3+} increases, the absorption peaks remain approximately the same; however the $5d$ bands broaden, and the onset of the lowest $5d$ band drops. Presumably this additional broadening is due to ion-ion interactions. Elias *et al.* [8], showed that the $5d$ band begins at ~ 35000 cm^{-1} in pure CeF_3 at 100 K. The lowest $5d$ absorption band does not begin abruptly with a zero-phonon line, but gradually. The peaks in the absorption of the $5d$ levels measured in a thin single crystal film of CeF_3 at room temperature are given in Table 1 [11].

CeF_3 is birefringent. Laiho and Lakkisto have measured the dispersion of the ordinary and extraordinary indices of refraction from the visible to the near ultraviolet [13]. At 476 nm, n_o = 1.6258 and n_e = 1.6189. Measurements of the nonlinear index of refraction range from 1.3 to 1.55 × 10^{-13} esu at 1.06 μm [14, 15].

III. The Resonant and the Nonresonant Susceptibility

The CARS signal is proportional to the square of the third-order susceptibility tensor, $|\chi^{(3)}_{ijkl}|^2$. The tensor may be divided into a resonant (frequency dependent) and a nonresonant (frequency independent) part:

$$\chi^{(3)}_{ijkl} = \chi^{(3)R}_{ijkl} + \chi^{(3)NR}_{ijkl} \qquad (1)$$

The resonant part, $\chi^{(3)R}_{ijkl}$, is a complex quantity which contains the spectroscopic information. The nonresonant part, $\chi^{(3)NR}_{ijkl}$, is due to the bulk crystal, and is a real number.

A. The Resonant Susceptibility

For the CARS measurements with visible lasers, a frequency-doubled Nd^{3+}:YAG laser provides $\omega_2/2\pi c = 18794.3$ cm^{-1}. A tunable laser operating in the 21000 cm^{-1} region provides ω_1. The CARS signal at $\omega_3 = 2\omega_1 - \omega_2$ is then in the $\omega_3/2\pi c \approx 23200$ cm^{-1} region. (See Figure 1.) The magnitude of the resonant third-order susceptibility tensor peaks when $\hbar(\omega_1 - \omega_2)$ is equal to $\hbar\omega_R$, the energy of the Raman transition. In the appendix, the maximum value of $|\chi^{(3)R}_{zzzz}(-\omega_3, \omega_1, \omega_1, -\omega_2)|$, is calculated using the Axe theory of two-photon processes. This calculation is based on the following assumptions:

- The $5d$ intermediate states are the dominant intermediate states for the calculation of the Raman tensor. Additionally, the $5d$ intermediate states are treated as if all have the same energy (following the work of Judd [17], Ofelt [18] and Axe [16]). An average value of the measured $5d$ levels listed in Table 1 ($\omega_{5d}/2\pi c = 45000$ cm^{-1}) is used.
- The $4f$ levels are treated in the zero crystal field limit, meaning that the states have spherical (*i. e.* atomic) symmetry.
- The quantity $\langle 4f | r | 5d \rangle$ is derived from oscillator strength measurements in Ce^{3+}:LaF_3.

In addition, the methods used in the appendix are also used to calculate the total spontaneous electronic Raman cross section, σ_{zz}. (The indices correspond to the polarizations of the incident and scattered light, respectively.)

The results given in the the appendix show that for a CARS resonance between the ground state of the $^2F_{5/2}$ manifold and one of the four Stark components of the $^2F_{7/2}$ manifold, the maximum of resonant third-order susceptibility is

$$|\chi^{(3)R}_{zzzz}|_{max} \; (^2F_{5/2} \leftrightarrow {}^2F_{7/2}) \approx \frac{1.3 \times 10^{-14} \text{ esu}}{\Gamma'} \qquad (2)$$

where Γ' is the linewidth (HWHM) of the Raman transition in cm^{-1}. The linewidths for electronic Raman transitions between Stark components in rare earth crystals at low temperature should range from about 0.5 to 10 cm^{-1}. The lowest (metastable) level in a manifold usually has the smallest linewidth. As discussed earlier [3], the value in equation (2) is on the high end for electronic CARS in fully concentrated rare earth crystals.

B. The Nonresonant Susceptibility

In a CARS experiment the nonresonant susceptibility is responsible for the constant background in the signal. The nonresonant susceptibility is related to the product of the linear (n) and nonlinear (n_2) indices of refraction [26]:

$$\chi^{(3)NR}_{zzzz}(-\omega_3, \omega_1, \omega_1, -\omega_2) \approx \chi^{(3)NR}_{zzzz}(-\omega_1, \omega_1, \omega_1, -\omega_1) = \frac{n(\omega_1)\, n_2(\omega_1)}{12\pi} \qquad (3)$$

Using the data of Ref. [13] for n and that of Refs. [15] and [14] for n_2 yields $\chi^{(3)NR} = 6.1 \times 10^{-15}$ esu at 1.06 μm. The quantity $\chi^{(3)NR}$ is slightly dispersive, and changes (slowly) with increasing frequency. Sheik-Bahae, *et al.* [27] have shown that the dispersion of n_2 is a consequence of two-photon absorption to the crystal band gap, just as the dispersion of n is a consequence of single photon absorption. They applied a Kramers-Kronig analysis to a two-parabolic-band model to arrive at

$$n_2 \propto \frac{G_2(\hbar\omega / E_g)}{nE_g^4} \qquad (4)$$

where

$$G_2(x) = \frac{-2 + 6x - 3x^2 - \frac{3}{4}x^4 - \frac{3}{4}x^5 + 2(1 - 2x)^{3/2}\Theta(1 - 2x)}{64x^6} \tag{5}$$

E_g is the energy of the crystal band gap, and Θ is the unit step function. Empirically, they have shown that this model is applicable to a wide range of solids, from wide-gap insulating crystals to semiconductors. One may be tempted to use the energy of the $4f \rightarrow 5d$ band gap in CeF_3 as E_g. However, $4f \rightarrow 5d$ two-photon absorption is forbidden in first order since $\Delta l = 1$. Gayen *et al.* have measured the $4f \rightarrow 5d$ two-photon absorption cross section of Ce^{3+} in CaF_2 [28]. If one assumes that the $4f \rightarrow 5d$ two-photon cross section of Ce^{3+} in CeF_3 is similar to Ce^{3+} in CaF_2, then the two-photon absorption contribution to n_2 due to the Ce^{3+} $4f \rightarrow 5d$ band gap should be negligible. Ultraviolet reflectance spectra show the onset of the valence band to conduction band transition at ~ 10 eV in CeF_3 [11]. (LaF_3, which has nearly the same linear and nonlinear refractive indices as CeF_3 [13–15], also shares nearly identical optical properties in the 8 – 34 eV range.) Using E_g = 10 eV, and the measured value of n_2 at 1.06 μm, $\chi^{(3)NR}$ has the following values in the following spectral regions:

9397 cm^{-1}	(1.06 μm)	$\chi^{(3)NR}_{zzzz} = 6.1 \times 10^{-15}$ esu
21000 cm^{-1}	(476 nm)	$\chi^{(3)NR}_{zzzz} = 8.0 \times 10^{-15}$ esu
28192 cm^{-1}	(355 nm)	$\chi^{(3)NR}_{zzzz} = 9.7 \times 10^{-15}$ esu

Therefore, one may expect from equation (2) a figure of merit of $C = |\chi^{(3)R}/\chi^{(3)NR}|_{max} \approx 2$ in the visible region if the linewidths are about 1 cm^{-1}. While there is

some uncertainty in this figure, one can expect that electronic CARS resonances in CeF_3 at low temperature should be readily observable.

IV. Experimental

The experimental apparatus is very similar to that described in a previous paper [3]. The CeF_3 crystal, obtained from Optovac, Inc., is a 1 cm^3 polished cube with the crystal axis parallel to the faces. In order to minimize thermal broadening of the Stark components, an Oxford CF1204 helium gas flow cryostat cooled the CeF_3 crystal to 3.8 K.

CARS resonances in the visible region used the Nd^{3+}:YAG laser second harmonic (18794.3 cm^{-1}, linewidth = 0.52 cm^{-1} (FWHM)) to provide ω_2. Frequency-tripled light from the same laser pumped a dye laser operating with Coumarin 500 (~ 21000 cm^{-1}, linewidth = 0.25 cm^{-1}) to provide a variable ω_1. At each laser shot, the signal is normalized to the square of the intensity of beam ω_1. The energy of each beam was about 100 μJ/pulse. Both ω_1 and ω_2 were polarized parallel to the optical (z) axis of CeF_3. The optimal signal was seen when the angle between ω_1 and ω_2 was ~ 50 mrad. This yielded measurements of $|\chi^{(3)}_{zzzz}|^2$. Figures 2 and 3 show CARS resonances at $(\omega_1 - \omega_2)/2\pi c$ = 2161 cm^{-1} and 2239 cm^{-1}, respectively. A measure of the success of this experiment is that it now makes sense to plot the data on a logarithmic intensity scale. In Figure 2, the normalized intensity ranges from 0.09 to 9.5 for a dynamic range of about 10^2. (The dynamic range for previous electronic CARS measurements in pure rare earth crystals did not exceed 2 [1, 2].) CARS resonances involving the two highest Stark components of the $^2F_{7/2}$ manifold were not observed. This is probably due to the large linewidths of these levels.

CARS resonances were also detected using ultraviolet laser frequencies. The frequency tripled light from the Nd^{3+}:YAG laser at $\omega_1/2\pi c$ = 28191.5 cm^{-1} provided one

beam, and also pumped a dye laser to provide tunable radiation in the $\omega_2/2\pi c \approx 26000$ cm^{-1} range. The linewidths of the lasers were $\Delta\omega_1/2\pi c = 0.80$ cm^{-1} and $\Delta\omega_2/2\pi c = 0.60$ cm^{-1}. Again, measurements were taken with the polarizations of both ω_1 and ω_2 parallel to the z axis to yield $|\chi^{(3)}_{zzzz}|^2$. These resonances are shown in Figures 4 and 5. Again, no resonances were observed for the two highest states of the $^2F_{7/2}$ manifold.

Additionally, measurements were made with the polarizations of ω_1 and ω_2 perpendicular to each other (*yzzy* and *yzzy*). These resonances were not as intense as the *zzzz* resonances, and are discussed further in Ref. [29].

V. Analysis

The data are fit to a third-order susceptibility :

$$\frac{\chi^{(3)R}_{iiii}}{\chi^{(3)NR}_{iiii}} = \frac{-A}{(\omega_1 - \omega_2 - \omega_R) - i\Gamma} \qquad (6)$$

where $\hbar\omega_R$ and Γ are the energy and Lorentzian (HWHM) linewidth of the Raman transition. In this notation, $C = |\chi^{(3)R}/\chi^{(3)NR}|_{max} = A/\Gamma$. A least squares fit is obtained using the quantities A and Γ as variable parameters. The finite bandwidths of the input lasers are taken into account by deconvolving the spectrum with the lineshapes of the incident lasers [30].

A best fit of the data in Figures 2 to 5 gives values for A, Γ and C given in Table 2. The fitted curves are drawn as solid lines in Figures 2 to 5.

Since the visible lasers have narrower linewidths than the ultraviolet lasers, they may be expected to yield better data. Additionally, since the magnitude of the nonresonant susceptibility is extrapolated from its value at 1.06 μm, the value of $\chi^{(3)NR}_{zzzz}$ is likely to be

more accurate for the visible frequencies. The dynamic range for the 2161 cm^{-1} resonance was much higher than the 2239 cm^{-1} resonance. As a result the 2161 cm^{-1} resonance may be expected to yield better data than the 2239 cm^{-1} resonance. The linewidths should be the same when measured with either laser setup. The difference in measured linewidths between the visible and ultraviolet spectra (0.55 and 0.60 cm^{-1} for the 2161 cm^{-1} resonance and 3.5 and 4.5 cm^{-1} for the 2239 cm^{-1} resonance) are indicative of the accuracy of the measurements. Estimated uncertainties in the data are included in Table 2.

Note that the peak CARS intensities are similar for 2161 cm^{-1} resonances. The ultraviolet spectrum has a greater figures of merit (C = 4.8) compared to the visible spectrum (C = 3.5). The ultraviolet spectra were recorded with broader linewidth lasers, and the effect is that the CARS peaks are suppressed to a greater degree than in the visible spectra which were recorded with narrower band lasers. The spectra do differ in the difference between maxima and minima. The difference between maxima, $(\omega_1 - \omega_2)_+$, and minima, $(\omega_1 - \omega_2)_-$, in the limit of zero-linewidth lasers is [31]:

$$[(\omega_1 - \omega_2)_+ - (\omega_1 - \omega_2)_-]^2 = A^2 + 4\Gamma^2 \qquad (7)$$

The ultraviolet resonances have a larger difference between peak and valley than do the visible resonances due to a larger value of A.

The linewidth of the higher lying level at 2239 cm^{-1} is much greater than the level at 2161 cm^{-1}. The higher state may decay to the lower state by the spontaneous emission of a single phonon and is lifetime broadened. This broadening is enhanced by the existence of a 78 cm^{-1} optical phonon in the CeF_3 crystal [32]. The lower level, on the other hand, requires the relatively unlikely simultaneous emission of several phonons to decay to the ground $^2F_{5/2}$ manifold. The $\Gamma/2\pi c$ = 0.55 cm^{-1} linewidth of the lower level is probably due to ion-ion interactions which occur in fully concentrated rare earth crystals.

The quantity $|\chi^{(3)R}|_{max}$ may be calculated from Table 2. For the experiment with visible lasers, $|\chi^{(3)R}|_{max} \cdot \Gamma' = 1.5 \times 10^{-14}$ esu for the 2161cm^{-1} resonance and 0.6×10^{-14} esu for the 2239 cm^{-1} resonance. These values agree quite well with the prediction of the Axe theory given in equation (2). Because the calculation in the appendix neglected crystal field effects, the value given in equation (2) is the *average* value of $|\chi^{(3)R}|_{max}$ for the four Stark components of the $^2F_{7/2}$ manifold.

The parameter A is related to the total spontaneous Raman cross section by

$$\sigma_{zz} = \frac{32\pi\hbar\omega_s^4}{Nc^4} A \ \chi_{zzzz}^{(3)NR} \tag{8}$$

where ω_s is the frequency of the scattered light (the Stokes frequency). The Raman cross sections (assuming $\omega_s = \omega_1$) are listed in Table 2. The Raman cross section in the visible region compares well with the estimated values in the appendix (equation (28)). The value in equation (28) is the *sum* of the Raman cross sections of the *four* levels of the $^2F_{7/2}$ manifold. The major uncertainty in the experimental values are due to the uncertainty in the nonresonant susceptibility (or equivalently, the nonlinear index of refraction). An accurate measurement of n_2 in CeF_3 in the z polarization in at 476 nm and 355 nm would allow a more accurate absolute Raman cross section measurement.

Assuming that the 5*d* levels are degenerate, and that the 5*d* configuration dominates the electronic Raman processes, the dispersion of the maximum value of the resonant susceptibility is given in equations (12) and (14) of the appendix:

$$\left|\chi_{zzzz}^{(3)R}(-\omega_3,\ \omega_1,\ \omega_1,\ -\omega_2)\right|_{max}$$
$$\propto \left[(\omega_3 - \omega_{5d})^{-1} - (\omega_1 + \omega_{5d})^{-1}\right]\left[(\omega_1 - \omega_{5d})^{-1} - (\omega_2 + \omega_{5d})^{-1}\right] \tag{9}$$

This allows a comparison of values of A for the visible and ultraviolet experiments. For the visible experiments, $\omega_1/2\pi c \approx 21000$ cm^{-1}, $\omega_2/2\pi c = 18794.3$ cm^{-1} and $\omega_3/2\pi c \approx 23200$ cm^{-1}. For the ultraviolet experiments, $\omega_1/2\pi c = 28191.5$ cm^{-1}, $\omega_2/2\pi c \approx 26000$ cm^{-1} and $\omega_3/2\pi c \approx 30400$ cm^{-1}. In the Axe approximation, $\omega_{5d}/2\pi c = 45000$ cm^{-1} which is the average of the $5d$ levels. (See Table 1.) Then

$$\frac{A_{\rm uv}}{A_{\rm vis}} = \frac{\chi^{(3)NR}_{\rm vis}}{\chi^{(3)NR}_{\rm uv}} \times \frac{\left[(\omega_3^{\rm uv} - \omega_{5d})^{-1} - (\omega_1^{\rm uv} + \omega_{5d})^{-1}\right]\left[(\omega_1^{\rm uv} - \omega_{5d})^{-1} - (\omega_2^{\rm uv} + \omega_{5d})^{-1}\right]}{\left[(\omega_3^{\rm vis} - \omega_{5d})^{-1} - (\omega_1^{\rm vis} + \omega_{5d})^{-1}\right]\left[(\omega_1^{\rm vis} - \omega_{5d})^{-1} - (\omega_2^{\rm vis} + \omega_{5d})^{-1}\right]}. \tag{10}$$

or, upon inserting the above values (along with the nonresonant susceptibilities)

$$\frac{A_{\rm uv}}{A_{\rm vis}} = 1.43 \pm 0.21 \tag{11}$$

The uncertainty in the above figure comes from the uncertainty in $\chi^{(3)NR}_{\rm vis}/\chi^{(3)NR}_{\rm uv}$. The experimental ratios, from Table 2, are $(A_{\rm uv}/A_{\rm vis})$ (2161 cm^{-1}) = 1.46±0.16 and $(A_{\rm uv}/A_{\rm vis})$ (2161 cm^{-1}) = 2.23±0.95. This agreement is quite good. In their analysis of the asymmetries in electronic Raman transitions in $ErPO_4$ and $TmPO_4$, Becker *et al.* [33] indicated that intermediate states of d and g electronic configurations make contributions of "equal significance." The above results indicate that the $5d$ configuration alone accounts for the dispersion of of $|\chi^{(3)R}|_{\rm max}$ in CeF_3.

VI. Summary

Strong electronic CARS resonances have been observed in CeF_3. Figures of merit, $C = |\chi^{(3)R}/\chi^{(3)NR}|_{max} = A/\Gamma$, are an order of magnitude larger than measured previously in other pure rare earth crystals. This is due to the fairly large electronic Raman cross section which is, in turn, due to the relatively low $5d$ configuration of the Ce^{3+} ion. The absolute strengths of these resonances were accurately predicted using the Axe theory of two-photon processes with $4f \rightarrow 5d$ absorption data. Approximating the intermediate states by a single degenerate $5d$ level at 45000 cm^{-1} accounted for both the absolute magnitude and dispersion properties of $|\chi^{(3)R}|_{max}$.

VII. Acknowledgements

The author acknowledges helpful discussions with Norman Edelstein, Lloyd Chase, Wing Kot, Douglas Hamilton, E. Van Stryland and Sumner Davis. Rob Sparrow of Optovac, Inc. (North Brookfield, Massachusetts) supplied the CeF_3 crystal used in this work. This research was supported by the Director, Office of Energy Research, Office of Basic Energy Sciences, Chemical Science Division, the U. S. Department of Energy, under Contract No. DE–AC03–76SF00098.

Appendix: Calculation of $|\chi^{(3)R}|_{max}$ and σ_{zz}

A. Application of the Axe Theory of Two-photon Processes

The quantity $|\chi^{(3)R}_{zzzz}|_{max}$ is calculated for an electronic CARS experiment in CeF_3 using visible lasers. A frequency-doubled Nd^{3+}:YAG laser provides $\omega_2/2\pi c$ = 18794.3 cm^{-1}. A tuneable laser operating in the 21000 cm^{-1} region provides ω_1. The CARS signal at $\omega_3 = 2\omega_1 - \omega_2$ is then in the $\omega_3/2\pi c \approx 23200$ cm^{-1} region. (See Figure 1.) The quantity $|\chi^{(3)R}_{zzzz}(-\omega_3, \omega_1, \omega_1, -\omega_2)|_{max}$ for singly resonant CARS may be derived from [31, 34]

$$|\chi^{(3)R}_{iiii}|_{max} = \frac{N\Lambda\,|\alpha_{ii}(\omega_3, \omega_1)\alpha_{ii}(\omega_1, \omega_2)|}{12\hbar\Gamma} \tag{12}$$

where

$$\alpha_{uv}(\omega_x, \omega_y) = \frac{1}{\hbar}\sum_n \left[\frac{\langle g\ |er_u|\ n\rangle\langle n\ |er_v|\ f\rangle}{(\omega_x - \omega_{gn})} - \frac{\langle g\ |er_v|\ n\rangle\langle n\ |er_u|\ f\rangle}{(\omega_y + \omega_{gn})}\right] \tag{13}$$

is the usual (nonresonant) Raman tensor. The kets $|g\rangle$, $|f\rangle$, and $|n\rangle$ correspond to the ground, low lying, and intermediate states with energies zero, $\hbar\omega_{gf}$, and $\hbar\omega_{gn}$. The number density of scatterers is N, and Γ is the Lorentzian linewidth (HWHM) of the $|g\rangle \rightarrow |f\rangle$ transition. The experiment determines the linewidth, Γ, but for the purposes of calculation we use $\Gamma/2\pi c$ = 1 cm^{-1}. The term $\Lambda = ((n^2 + 2)/3)^4$, where n is the refractive index, contains the local field corrections.

The first approximation is the assumption that the intermediate states, $|n\rangle$, are dominated by the $5d$ levels at $\omega_{gn}/2\pi c \approx$ 40000 to 50000 cm^{-1}. (See Table 1.) Other excited states of opposite parity are presumed to be too high in energy to contribute

appreciably. The next approximation is originally due to Judd [17] and Ofelt [18], and was first applied to two-photon processes by Axe [16]. If the denominators do not cause the quantities in the summation to change rapidly as a function of n, the denominators may be removed from the summation. This is equivalent to setting the energies of all the $5d$ levels to the same energy. That is, $\omega_{gn}/2\pi c \equiv \omega_{5d}/2\pi c \equiv 45000\ \text{cm}^{-1}$. Equation (13) may now be written as

$$\alpha_{ii}(\omega_x, \omega_y) = \frac{e^2}{\hbar}\left[\frac{1}{(\omega_x - \omega_{5d})} - \frac{1}{(\omega_y + \omega_{5d})}\right] \sum_{\text{all } 5d \text{ states}} \langle g \ |r_i| \ 5d\rangle\langle 5d \ |r_i| \ f\rangle \tag{14}$$

The initial and final states are in the $4f$ configuration and the intermediate states are $5d$. Using the methods of Axe [16], the above summation simplifies to

$$\sum_{\text{all } 5d \text{ states}} \langle 4f \ \psi JM \ |z| \ 5d\rangle\langle 5d \ |z| \ 4f \ \psi' J'M'\rangle$$

$$= \ \langle l = 3 \ ||\mathbf{C}^{(1)}|| \ l = 2\rangle^2 \ |\langle 4f \ | \ r \ | \ 5d\rangle|^2$$

$$\times \sum_{\lambda = 0,2} (2\lambda + 1) \begin{pmatrix} 1 & \lambda & 1 \\ 0 & 0 & 0 \end{pmatrix} \begin{Bmatrix} 1 & \lambda & 1 \\ 3 & 2 & 3 \end{Bmatrix} \langle 4f\psi JM \ |U_0^{(\lambda)}| \ 4f\psi' J'M'\rangle \tag{15}$$

The above equation may be evaluated if angular wavefunctions are available for both the initial and final states, and the quantity $|\langle 4f \ | \ r \ | 5d \ \rangle|$ is known. Unfortunately, the $4f - 5d$ radial overlap varies from crystal to crystal, and accurate angular wavefunctions for Ce^{3+} in CeF_3 (or LaF_3) are not known. As demonstrated below, an effective measure of $|\langle 4f \ | \ r \ | 5d \ \rangle|$ may be derived from the $4f \rightarrow 5d$ absorption spectrum of Ce^{3+} in LaF_3. For the $4f$ wavefunctions, those of the free Ce^{3+} ion are used.

B. Calculating $|\langle 4f | r | 5d \rangle|$ for Ce^{3+} in CeF_3

In the crystal field model, the crystal field Hamiltonian acts only upon angular variables. The radial wavefunctions are presumed to be unaffected by the crystal field interaction. However, studies [20, 22, 35–37] indicate that the *5d* radial wavefunction may be sensitive to the local crystal environment, and the quantity $|\langle 4f | r | 5d \rangle|$ can vary considerably from crystal to crystal. The *4f* wavefunction has no radial node while the *5d* radial wavefunction has two nodes, one near the maximum of the *4f* radial wavefunction. Since the interaction of the the *5d* electron with the host lattice is much greater than the *4f* electron, a small change in the *5d* radial wavefunction can significantly alter the radial overlap. Therefore, a calculation of $|\langle 4f | r | 5d \rangle|$ from the free ion wavefunctions cannot be applied to this work. An effective measurement of $|\langle 4f | r | 5d \rangle|$ may be derived from the *4f* $\rightarrow$ *5d* oscillator strength of the Ce^{3+} ion in the $(Ce,La)F_3$ environment.

The oscillator strength, *f*, is related to the absorption coefficient, *a*, by [38]

$$f = \frac{mc^2}{\pi e^2 N} \int a(\sigma)\, d\sigma \tag{16}$$

where $\sigma = 1/\lambda$. The oscillator strength is related to the dipole matrix element between the initial state $|i\rangle$ and final state $|f\rangle$ by [17]

$$f = \frac{2m\omega}{\hbar} \frac{(n^2 + 2)^2}{9n} |\langle i | \mathbf{r} | f \rangle|^2 \tag{17}$$

Both Ehrlich *et al.* [12] and Elias *et al.* [7] have measured the ultraviolet absorption spectra of Ce^{3+}:LaF_3. Integration of the total spectra according to equation (16) yields a total oscillator strength for the ground state to *5d* configuration transition. The oscillator strength should not depend on Ce^{3+} concentration, so that the Ce^{3+}:LaF_3 values should

apply to CeF_3. Ehrlich *et al.* measured the spectra of 0.05 mol % Ce^{3+} in LaF_3 at room temperature. Measurement of the area under the $4f \rightarrow 5d$ absorption spectrum gave $f = 2.2 \times 10^{-2}$. Elias *et al.* measured the absorption spectra of 0.01 mol % Ce^{3+} in LaF_3 at 100 K. The area under the spectrum gave $f = 1.8 \times 10^{-2}$, and there was no polarization dependence. For the purposes of this calculation, we shall assume that all levels of the $^2F_{5/2}$ manifold contribute equally to the absorption spectrum to give a $4f \rightarrow 5d$ oscillator strength of $f = 2 \times 10^{-2}$. From equation (17) and $f = 2 \times 10^{-2}$

$$\sum_{\text{all } 5d \text{ states}} |\langle i \mid z \mid 5d \rangle|^2 = 9.1 \times 10^{-19} \text{cm}^2 \tag{18}$$

Since all levels of the $^2F_{5/2}$ manifold are assumed to be equally occupied, the initial state is

$$|i\rangle = |^2F_{5/2}\rangle = \frac{1}{\sqrt{6}} {}^2F \left(|5/2, \pm 5/2\rangle + |5/2, \pm 3/2\rangle + |5/2, \pm 1/2\rangle \right) \tag{19}$$

and the small amount of J-mixing is ignored. The summation in equation (18) may be calculated with the aid of equation (15) and the quantities $\langle 3 \| C^{(1)} \| 2 \rangle = 3^{1/2}$, and

$$\langle 4f\ \psi JM \left| U_0^{(0)} \right| 4f\ \psi' J'M' \rangle = \frac{1}{\sqrt{7}} \delta(\psi JM,\ \psi' J'M') \tag{20}$$

to give

$$\sum_{\text{all } 5d \text{ states}} |\langle i \mid z \mid 5d \rangle|^2 = \frac{1}{7} |\langle 4f \mid r \mid 5d \rangle|^2 \tag{21}$$

(The $\lambda = 2$ term in equation (15) is zero when summed over all M.) Judd [39] has derived an equivalent result. Combining equation (18) with (21) gives

$$|\langle 4f\,|r|\,5d\rangle| = 0.25\ \text{Å} \qquad (22)$$

This compares with a value calculated for the free ion radial wavefunctions of $|\langle 4f|r|5d\rangle| =$ 0.441 Å [21].

C. Wavefunctions for Ce^{3+} in CeF_3

Accurate wavefunctions for the electronic states of the $4f$ configuration of the Ce^{3+} ion in CeF_3 are not available. Fourteen crystal field parameters are needed to characterize the Stark splitting of a $4f$ electron at a site of C_2 symmetry. Crystal field parameters are determined by a least squares fit of the energy levels to the crystal field Hamiltonian, and the angular wavefunctions are the eigenstates of the Hamiltonian. In the case of Ce^{3+}, the seven energy levels of the $4f$ configuration are insufficient to uniquely determine the fourteen crystal field parameters. Additionally, as discussed earlier, the only well determined energy levels of the $4f$ configuration are the the four Stark components of the $^2F_{7/2}$ manifold. Attempts to model the Ce^{3+}:LaF_3 crystal field by assuming a higher symmetry such as C_{2v} or D_{3h} (which decreases the number of crystal field parameters), have proven unsatisfactory [6].

Without wavefunctions of the initial and final states, equation (15) cannot be exactly solved. Approximations are necessary. As before, we assume that there is no J-mixing. For $4f$ electrons, a weak crystal field only mixes the J character of the $4f$ levels slightly. Additionally, we assume that the wavefunctions of the Stark components have spherical (*i. e.* atomic) symmetry as in the free ion. This is equivalent to a zero crystal field approximation. Thus,

$$|^2F_{5/2}\rangle = \frac{1}{\sqrt{6}}\,{}^2F\,(|5/2, \pm 5/2\rangle + |5/2, \pm 3/2\rangle + |5/2, \pm 1/2\rangle) \tag{23a}$$

$$|^2F_{7/2}\rangle = \frac{1}{\sqrt{8}}\,{}^2F\,(|7/2, \pm 7/2\rangle + |7/2, \pm 5/2\rangle + |7/2, \pm 3/2\rangle + |7/2, \pm 1/2\rangle) \tag{23b}$$

The zero crystal field approximation is likely to be better for a Ce^{3+} ion at a site of low symmetry (such as C_2) than at a site of high symmetry. Like the free ion wavefunctions, the angular wavefunction for a Stark component of a low symmetry ion will contain all M ($|M| \leq J$) values, and no selection rules exist. Additionally, the crystal field has only a second-order influence on the electronic Raman process. That is, the crystal field is responsible for the distribution of Raman intensity among the Stark components of a given manifold. Use of equation (15), $\langle {}^2F_{5/2} \| \mathbf{U}^{(2)} \| {}^2F_{7/2} \rangle = 0.350$, the Wigner-Eckart theorem, and the orthogonality relation,

$$\sum_{m_1, m_2} \begin{pmatrix} j_1 & j_2 & k \\ m_1 & m_2 & q \end{pmatrix} \begin{pmatrix} j_1 & j_2 & k' \\ m_1 & m_2 & q' \end{pmatrix} = \frac{1}{(2k+1)} \delta(k, k') \delta(q, q') \tag{24}$$

gives

$$\left| \sum_{\text{all } 5d \text{ states}} \langle {}^2F_{5/2} \mid z \mid 5d \rangle \langle 5d \mid z \mid {}^2F_{7/2} \rangle \right|^2 = 6.06 \times 10^{-3} \; |\langle 4f \mid r \mid 5d \rangle|^4 \tag{25}$$

Now the quantity $|\chi^{(3)R}_{zzzz}|_{max}$ may be estimated for ${}^2F_{5/2} \leftrightarrow {}^2F_{7/2}$ Raman transitions. Use of equations (12), (14), (22) and (25) gives $|\chi^{(3)R}_{zzzz}|_{max} = 5.1 \times 10^{-14}$ esu. This value is actually the sum of $|\chi^{(3)R}_{zzzz}|_{max}$ for the four Stark components of the ${}^2F_{7/2}$ manifold (if one

assumes that each level has a linewidth $\Gamma/2\pi c = 1\ \text{cm}^{-1}$). One might then expect that for each Stark level

$$|\chi^{(3)R}_{zzzz}|_{\max}\ (^2F_{5/2} \leftrightarrow {}^2F_{7/2}) \approx \frac{5.1 \times 10^{-14}\ \text{esu}}{4 \times (\text{HWHM linewidth in cm}^{-1})} \qquad (26)$$

This value is on the high end of resonant susceptibilities for singly resonant electronic CARS experiments in rare earth crystals [3].

D. Calculation of the Raman Cross Section

The above analysis also applies to the calculation of the total spontaneous Raman cross section for transitions from the $^2F_{5/2}$ ground state to the Stark levels of the $^2F_{7/2}$ manifold. The total (not differential) Raman cross section is related to the Raman in tensor equation (13) by

$$\sigma_{zz} = \frac{8\pi\Lambda\omega_s^4\,|\alpha_{zz}|^2}{3c^4} \qquad (27)$$

where ω_s is the frequency of scattered light (the Stokes frequency). This leads to a Raman cross section of (assuming $\omega_s/2\pi c = 21000\ \text{cm}^{-1}$)

$$\sigma_{zz}(^2F_{5/2} \leftrightarrow {}^2F_{7/2}) = 1.6 \times 10^{-29}\text{cm}^2 \qquad (28)$$

Again, the above expression is the *sum* of Raman cross sections for the *four* Stark components of the $^2F_{7/2}$ manifold. This is on the high end of the range of electronic Raman cross sections in rare earth crystals [40]. For comparison, Williams *et al.* [22, 36] measured $\sigma_{zz} = 1.4 \times 10^{-29}\ \text{cm}^2$ for the four $^2F_{7/2}$ Stark components in Ce^{3+}:$LuPO_4$.

References

[1] M. L. Shand, J. Appl. Phys. **52**, 1470 (1981).

[2] K. P. Traar, Phys. Rev. B **35**, 3111 (1987).

[3] D. Piehler and N. Edelstein, Phys. Rev. A **41**, 6406 (1990).

[4] J. H. VanVleck and M. H. Hebb, Phys. Rev. **46**, 17 (1934).

[5] R. A. Buchanan, H. E. Rast and H. H. Caspers, J. Chem. Phys. **44**, 4063 (1966).

[6] H. Gerlinger and G. Schaak, Phys. Rev. B **33**, 7438 (1986).

[7] L. R. Elias, W. S. Heaps and W. M. Yen, Phys. Rev. B **8**, 4989 (1973).

[8] L. R. Elias, R. Flach and W. M. Yen, Appl. Opt. **12**, 138 (1973).

[9] W. S. Heaps, L. R. Elias and W. M. Yen, Phys. Rev. B **13**, 94 (1976).

[10] K. Y. Yang and J. A. DeLuca, Appl. Phys. Lett. **31**, 594 (1977).

[11] C. G. Olson, M. Piacentini and D. W. Lynch, Phys. Rev. B **18**, 5740 (1978).

[12] D. J. Ehrlich, P. F. Moulton and J. R. M. Osgood, Opt. Lett. **5**, 339 (1980).

[13] R. Laiho and M. Lakkisto, Phil. Mag. B **48**, 203 (1983).

[14] R. Adair, L. L. Chase and S. A. Payne, Phys. Rev. B **39**, 3337 (1989).

[15] D. Milman, M. J. Weber and A. J. Glass, Appl. Phys. Lett. **31**, 822 (1977).

[16] J. D. Axe, Phys. Rev. **136**, A42 (1964).

[17] B. R. Judd, Phys. Rev. **127**, 750 (1962).

[18] G. S. Ofelt, J. Chem. Phys. **37**, 511 (1962).

[19] M. C. Downer, in *Laser Spectroscopy of Solids II*, edited by W. M. Yen (Springer-Verlag, Berlin, 1989), p. 29.

[20] L. L. Chase and S. A. Payne, Phys. Rev. B **34**, 8883 (1986).

[21] G. M. Williams, N. Edelstein, L. A. Boatner and M. M. Abraham, Phys. Rev. B **40**, 4143 (1989).

[22] G. M. Williams, Ph.D. thesis, University of California at Berkeley (1988).

[23] A. Zalkin, D. H. Templeton and T. E. Hopkins, Inorg. Chem. **5**, 1466 (1966).

[24] A. K. Cheetham, B. E. F. Fender, H. Fuess and A. F. Wright, Acta Cryst. **B32**, 94 (1976).

[25] *Landolt-Bornsteion, Neue Serie*, edited by K. H. Hellwege (Springer-Verlag, Berlin, 1973).

[26] M. D. Levenson, IEEE J. Quantum Electron. **QE-10**, 110 (1974).

[27] M. Sheik-Bahae, D. J. Hagan and E. W. VanStryland, Phys. Rev. Lett. **65**, 96 (1990).

[28] S. K. Gayen, D. S. Hamilton and R. H. Bartram, Phys. Rev. B **28**, 3706 (1983).
[29] D. Piehler, Ph.D. thesis, University of California at Berkeley (1990).
[30] R. E. Teets, Opt. Lett. **9**, 226 (1984).
[31] Y. R. Shen, *The Principles of Nonlinear Optics* (Wiley, New York, 1984).
[32] R. P. Bauman and S. P. S. Porto, Phys. Rev. **161**, 842 (1967).
[33] P. C. Becker, N. Edelstein, B. R. Judd, R. C. Leavitt and G. M. S. Lister, J. Phys. C **18**, L1063 (1985).
[34] The factor of 12 is added to conform to the notation of Maker and Tehrune (Phys. Rev. **137**, A801 (1965)).
[35] W. F. Krupke, Phys. Rev. **145**, 325 (1966).
[36] G. M. Williams, P. C. Becker, J. G. Conway, N. Edelstein, L. A. Boatner and M. M. Abraham, Phys. Rev. B **40**, 4132 (1989).
[37] R. C. Powell, S. A. Payne, L. L. Chase and G. D. Wilke, Phys. Rev. B **41**, 8593 (1990).
[38] J. I. Steinfeld, *Molecules and Radiation* (MIT Press, Cambridge, Massachusetts, 1985).
[39] B. R. Judd, Inorg. Chim. Acta **139**, 341 (1987).
[40] A. Keil and S. P. S. Porto, J. Mol. Spectrosc. **32**, 458 (1969).

configuration		energy (cm^{-1})
		50400
		48400
$5d$ [a]		45600
		42300
		39900
		2860
	$^2F_{7/2}$	2640
		2239
$4f$ [b]		2161
		~ 280 [c]
	$^2F_{5/2}$	~ 160 [c]
		0

Table 1. Energy levels of the Ce^{3+} ion in CeF_3. (All levels have the same symmetry label.)

(a) Energy levels of the $5d$ configuration refer to the peaks of the absorption bands. Absorption for the lowest $5d$ band begins at ~ 35000 cm^{-1}. Energy levels for the $5d$ configuration are from Ref. [11].

(b) Energy levels for the $4f$ configuration are from Ref. [6].

(c) The states of the $^2F_{5/2}$ manifold are coupled to the near-resonant optical phonons, giving very broad vibronic states.

	$\omega_R/2\pi c$ (cm^{-1})	*iiii*	$A/2\pi c$ (cm^{-1})	$\Gamma/2\pi c$ (cm^{-1})	C [a]	σ_{zz} [b] (cm^2)
visible lasers $\omega_1/2\pi c \approx 21000\ cm^{-1}$ $\omega_2/2\pi c = 18794.3\ cm^{-1}$ $\chi^{(3)NR}_{zzzz} \approx$ $(8.0\pm2.0) \times 10^{-15}$ esu	2161	*zzzz*	1.95±0.10	0.55±0.03	3.5	$(5.0\pm1.1) \times 10^{-30}$
	2239	*zzzz*	0.72±0.22	3.5±1.0	0.21	$(1.9\pm0.7) \times 10^{-30}$
ultraviolet lasers $\omega_1/2\pi c = 28191.5\ cm^{-1}$ $\omega_2/2\pi c \approx 26000\ cm^{-1}$ $\chi^{(3)NR}_{zzzz} \approx$ $(9.7\pm2.9) \times 10^{-15}$ esu	2161	*zzzz*	2.85±0.29	0.60±0.06	4.8	$(2.9\pm0.9) \times 10^{-29}$
	2239	*zzzz*	1.6±0.5	4.5±1.4	0.36	$(1.6\pm0.7) \times 10^{-29}$

Table 2. Summary of the data and estimated uncertainties.

(a) $C = |\chi^{(3)R}_{ijji} / \chi^{(3)NR}_{ijji}|_{max} = A/\Gamma$

(b) The total spontaneous Raman cross section σ_{zz}, at $\omega_s = \omega_1$, is related to A and $\chi^{(3)NR}_{zzzz}$ through equation (8) .

Figure Captions

FIGURE 1. Schematic diagram of singly resonant electronic CARS in CeF_3 using visible lasers. A frequency doubled Nd^{3+}:YAG laser provides a fixed $\omega_2/2\pi c$ =18794 cm^{-1}. A tuneable dye laser provides $\omega_1/2\pi c \approx 21000$ cm^{-1}. Energy levels are not drawn to scale. Only the energy levels measured in this paper are drawn.

FIGURE 2. Intensity of CARS signal, normalized to the off resonance intensity, at frequency ω_3 as a function of $\omega_1 - \omega_2$ with the visible lasers polarized in the z direction. Solid line is a fit to the parameters listed in Table 2. ($A/2\pi c$ = 1.95 cm^{-1}, $\Gamma/2\pi c$ = 0.55 cm^{-1}) (a) Linear intensity scale. (b) Logarithmic intensity scale.

FIGURE 3. Intensity of CARS signal, normalized to the off resonance intensity, at frequency ω_3 as a function of $\omega_1 - \omega_2$ with the visible lasers polarized in the z direction. Solid line is a fit to the parameters listed in Table 2. ($A/2\pi c$ = 0.72 cm^{-1}, $\Gamma/2\pi c$ = 3.47 cm^{-1})

FIGURE 4. Intensity of CARS signal, normalized to the off resonance intensity, at frequency ω_3 as a function of $\omega_1 - \omega_2$ with the ultraviolet lasers polarized in the z direction. Solid line is a fit to the parameters listed in Table 2. ($A/2\pi c$ = 2.85 cm^{-1}, $\Gamma/2\pi c$ = 0.60 cm^{-1}) (a) Linear intensity scale. (b) Logarithmic intensity scale.

FIGURE 5. Intensity of CARS signal, normalized to the off resonance intensity, at frequency ω_3 as a function of $\omega_1 - \omega_2$ with the ultraviolet lasers polarized in the z direction. Solid line is a fit to the parameters listed in Table 2. ($A/2\pi c$ = 1.61 cm^{-1}, $\Gamma/2\pi c$ = 4.52 cm^{-1})

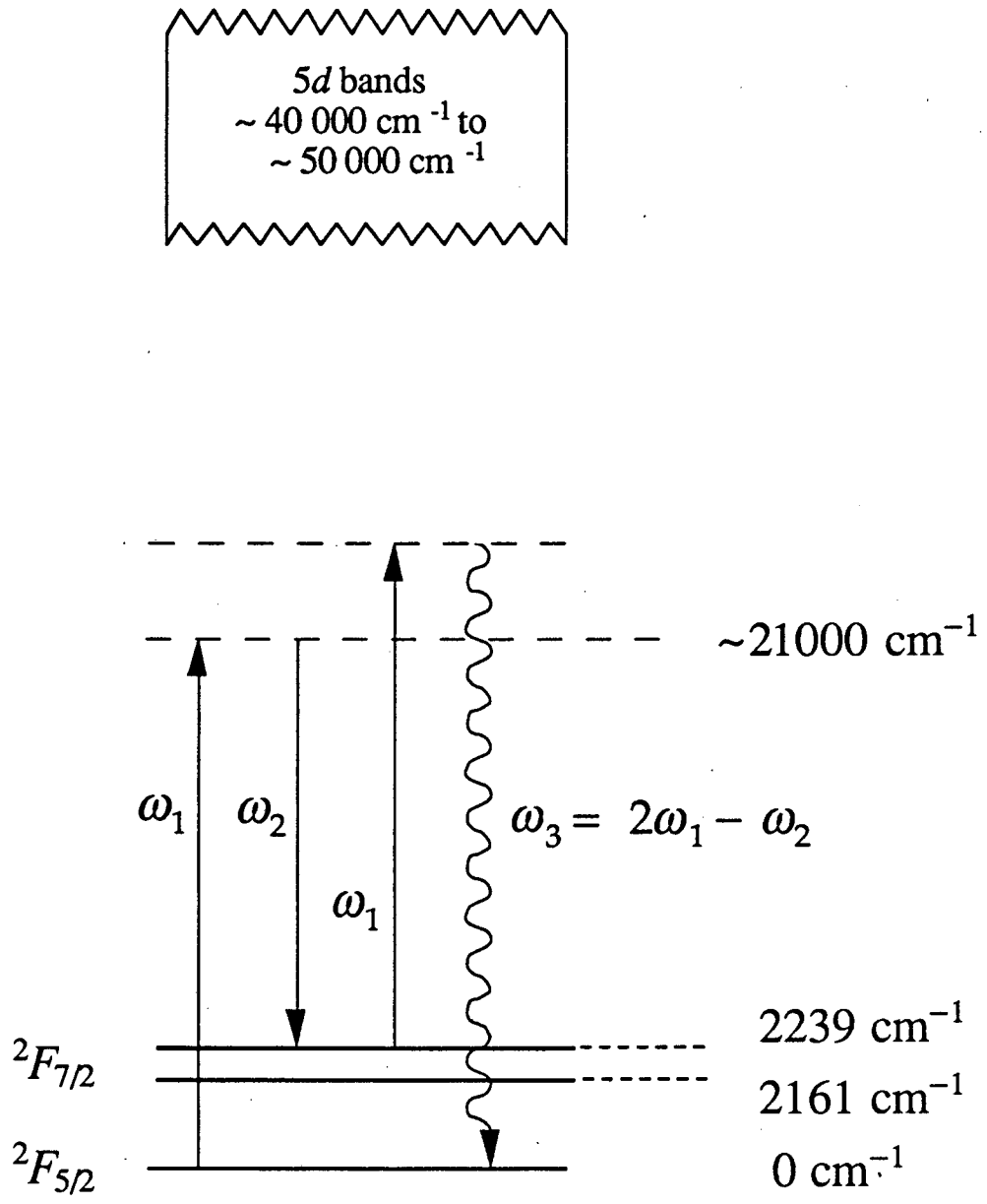
5d bands
~ 40 000 cm -1 to
~ 50 000 cm -1
~21000 cm−1
ω1
ω2
ω1
ω3 = 2ω1 − ω2
2239 cm−1
2161 cm−1
0 cm−1
2F7/2
2F5/2

Figure 1.

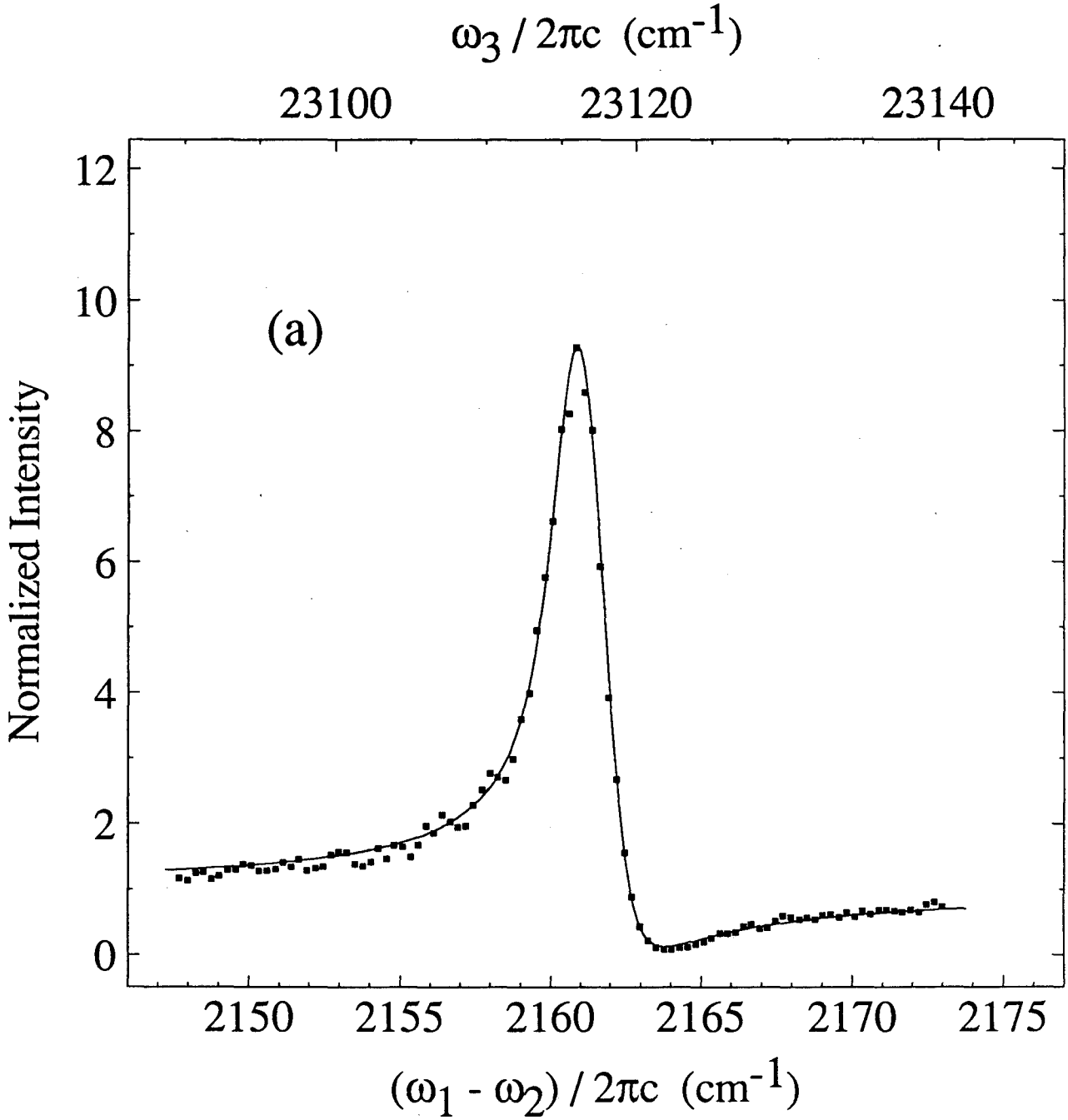
ω3 / 2πc (cm-1)
23100
23120
23140
12
10
8
6
4
2
0
(a)
Normalized Intensity
2150
2155
2160
2165
2170
2175
(ω1 - ω2) / 2πc (cm-1)

Figure 2(a).

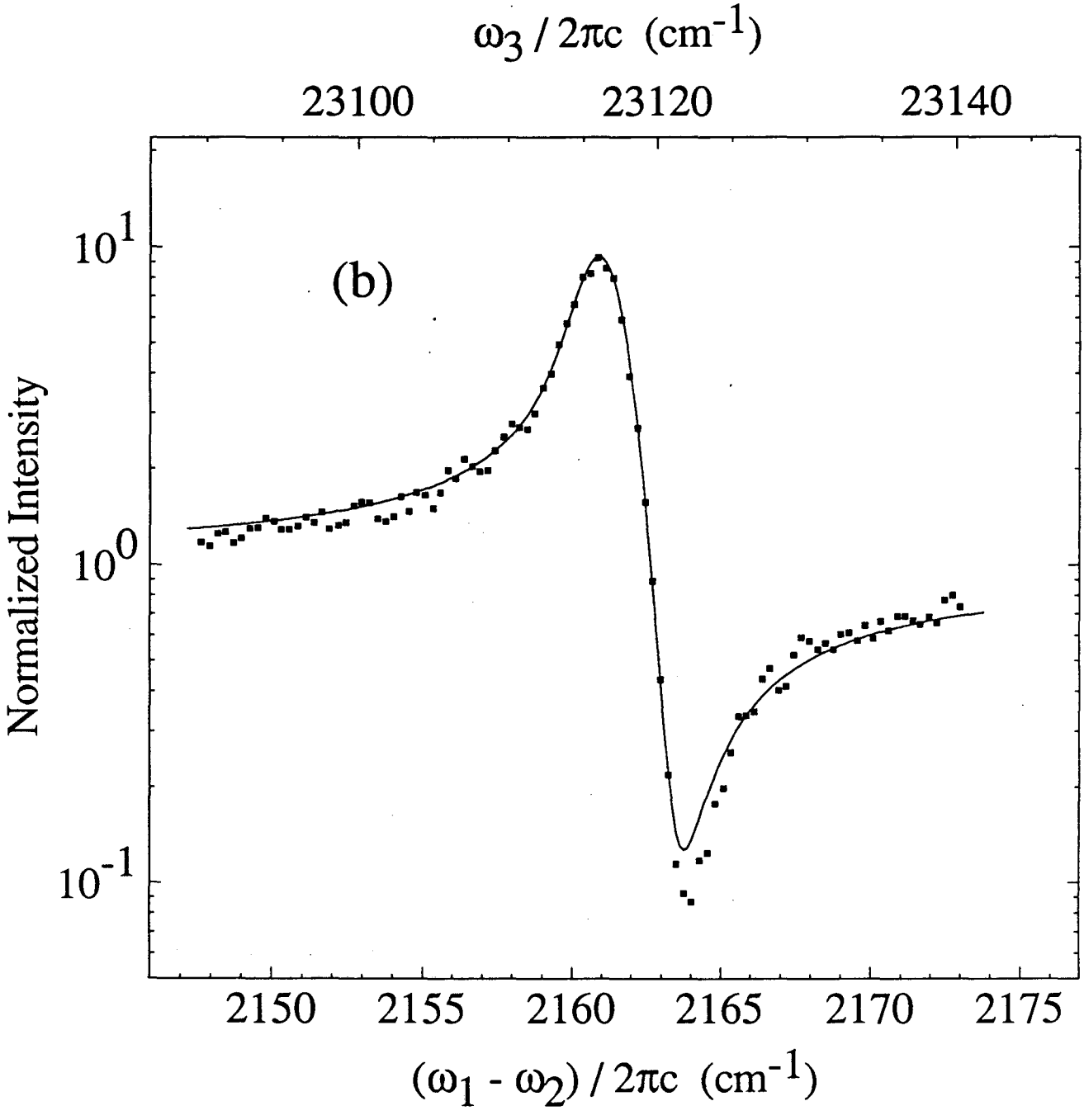
$\omega_3 / 2\pi c$ (cm^{-1})
23100
23120
23140
(b)
Normalized Intensity
10^1
10^0
10^{-1}
2150
2155
2160
2165
2170
2175
$(\omega_1 - \omega_2) / 2\pi c$ (cm^{-1})

Figure 2(b).

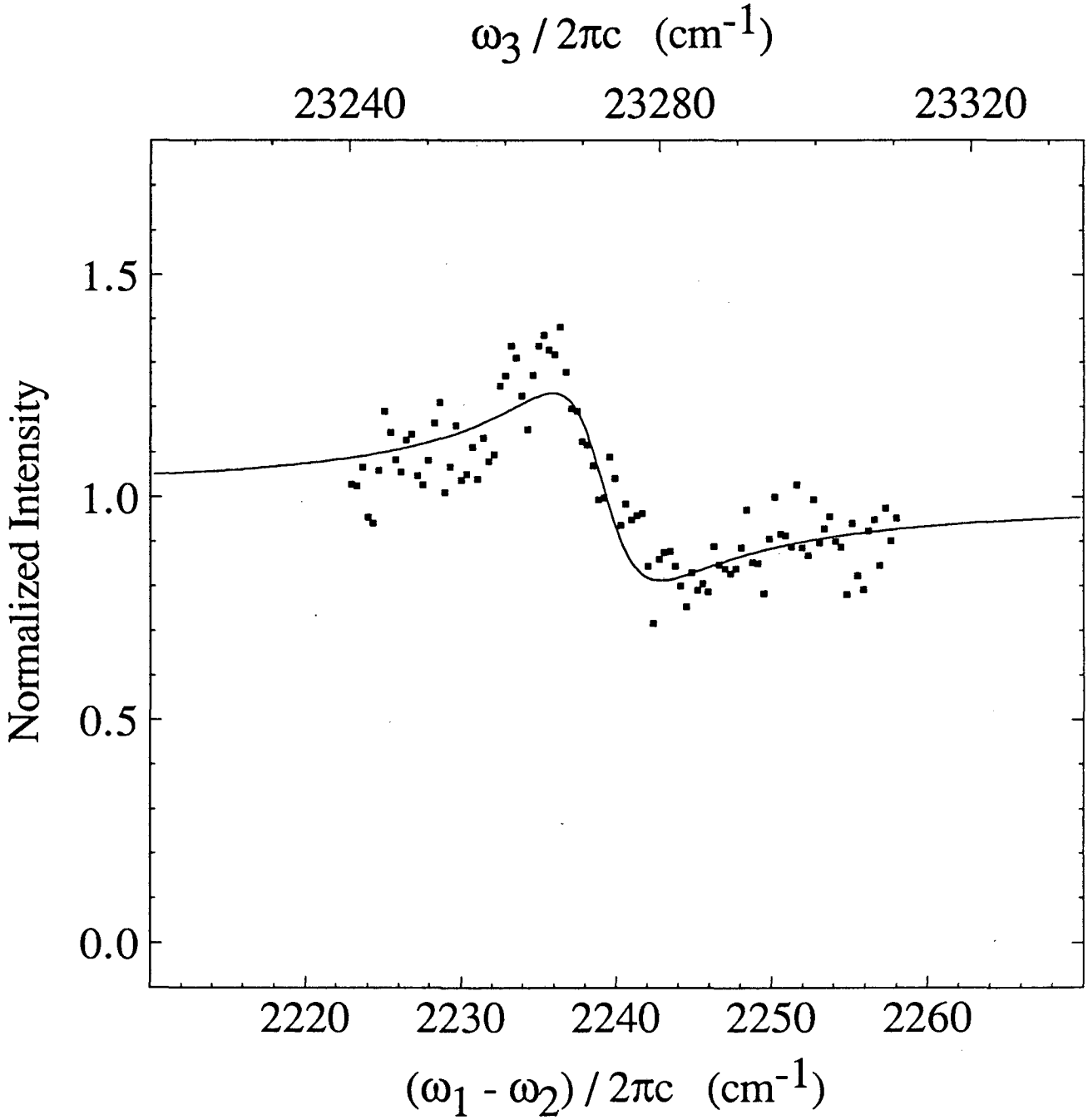
$\omega_3 / 2\pi c$ (cm^{-1})
23240
23280
23320
1.5
1.0
0.5
0.0
Normalized Intensity
2220
2230
2240
2250
2260
$(\omega_1 - \omega_2) / 2\pi c$ (cm^{-1})

Figure 3.

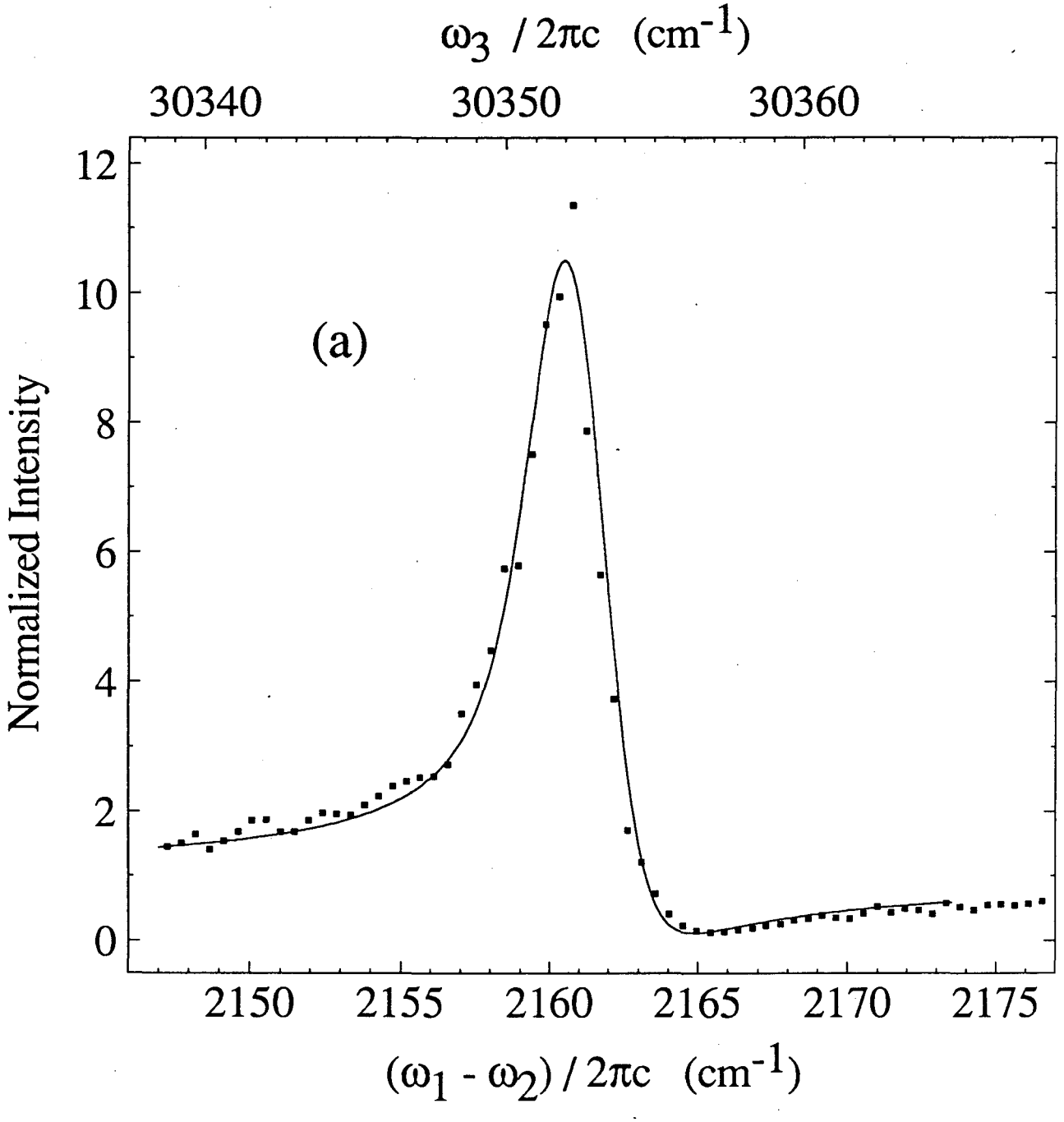
ω_3 / 2πc (cm^{-1})
30340
30350
30360
12
10
8
6
4
2
0
(a)
Normalized Intensity
2150
2155
2160
2165
2170
2175
(ω_1 - ω_2) / 2πc (cm^{-1})

Figure 4(a).

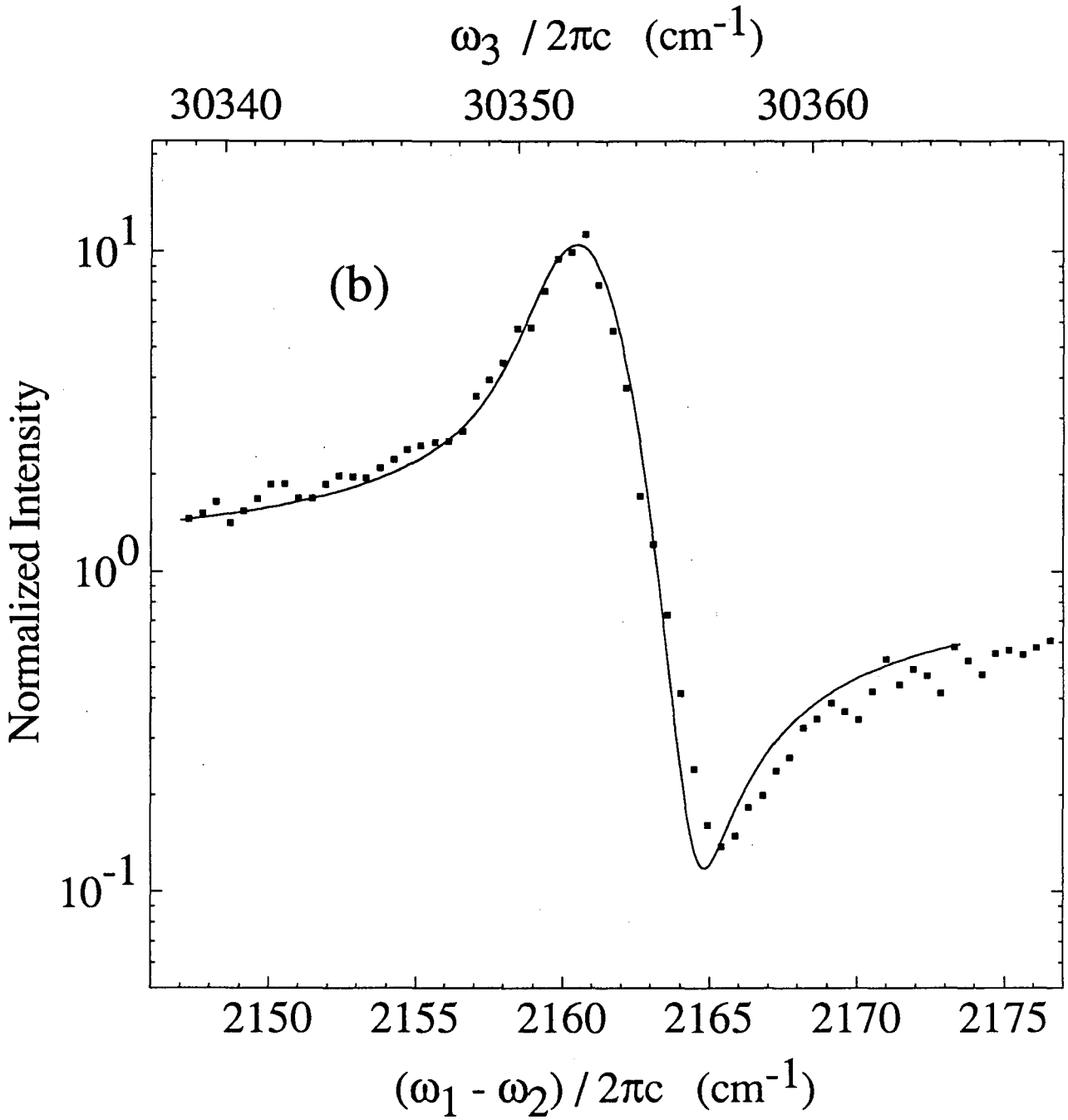
$\omega_3 / 2\pi c$ (cm^{-1})
30340
30350
30360
(b)
10^1
10^0
10^{-1}
Normalized Intensity
2150
2155
2160
2165
2170
2175
$(\omega_1 - \omega_2) / 2\pi c$ (cm^{-1})

Figure 4(b).

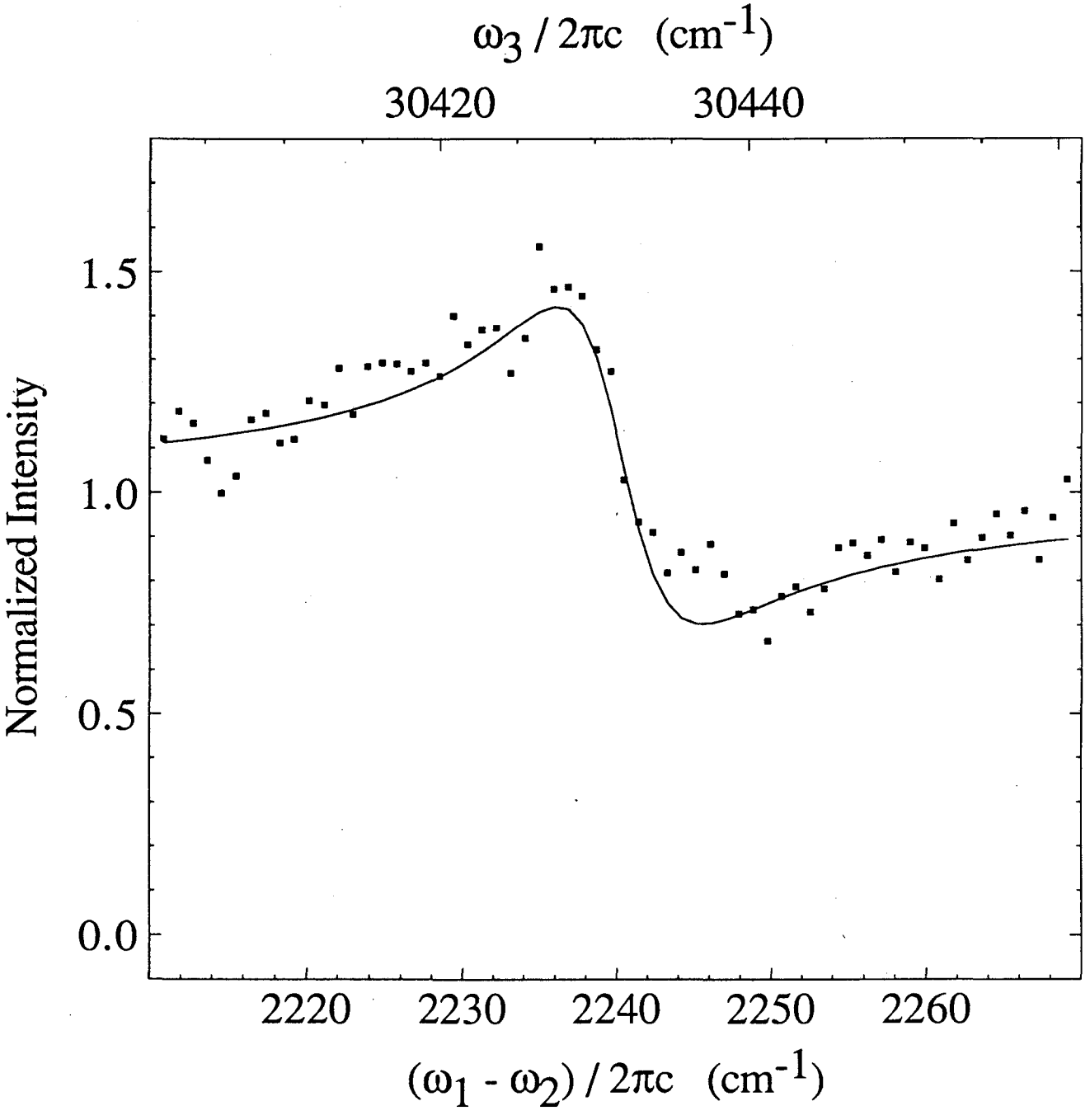
$\omega_3 / 2\pi c$ (cm^{-1})
30420
30440
Normalized Intensity
1.5
1.0
0.5
0.0
2220
2230
2240
2250
2260
$(\omega_1 - \omega_2) / 2\pi c$ (cm^{-1})

Figure 5.

LAWRENCE BERKELEY LABORATORY
UNIVERSITY OF CALIFORNIA
INFORMATION RESOURCES DEPARTMENT
BERKELEY, CALIFORNIA 94720